Optical Muscle Contraction Detection via Frequency Multiplexed LEDs

Sebastian Hauschild
Center of Excellence CoSA
Lübeck University of Applied Sciences
Lübeck, Germany
sebastian.hauschild@th-luebeck.de

Fabian John
Center of Excellence CoSA
Lübeck University of Applied Sciences
Lübeck, Germany
fabian.john@th-luebeck.de

Horst Hellbrück
Center of Excellence CoSA
Lübeck University of Applied Sciences
Lübeck, Germany
horst.hellbrueck@th-luebeck.de

Roman Kusche
Department of Computer Science
Hamburg University of Applied Sciences
Hamburg, Germany
roman.kusche@haw-hamburg.de

***Abstract*—In many biomedical applications, such as prosthesis control, but also in the field of human-computer interaction, muscle contraction detection plays a decisive role. Common principles are based on electrophysiological methods, like electromyography or impedance myography. Unfortunately, these principles require electrodes, which can cause skin irritations and lead to significant motion artifacts. This work presents an alternative method based on the optical characteristics of tissue, known as Optomyography (OMG). The fundamental idea is that the tissue between the skin surface and the muscle consists of multiple layers, each exhibiting distinct optical reflective properties. During a muscle contraction, the geometric structure of these layers changes and therefore also the reflective properties of an area under investigation are affected. To distinguish muscle contractions and motion artifacts, we apply two separate light sources with wavelengths of 850 nm and 630 nm to illuminate the tissue through the skin and an adjacent photodiode to detect the reflected amount of light. To enable the simultaneous measurement with both wavelengths, a self developed problem-specific approach is presented as an alternative to the time multiplexed method. This approach is based on frequency multiplexed LEDs as light sources, which are driven by voltage-controlled current sources. For evaluation, it is implemented as an electronic measurement system. After a characterization of this system, first subject measurements from the forearm are presented. These measurements demonstrate the ability of the system to detect muscle contractions optically.**

***Index Terms*—human-computer interaction, measurement system, muscle contractions, optical sensor, optomyography, photoplethysmography, prosthetics**

I. Introduction

In addition to conventional input devices, physiology can function as an interface between humans and technical systems by acquiring the corresponding biosignals. Due to the good controllability of muscle contractions, these in particular can be utilized for this purpose. For example, in upper limb prosthetics, muscles are often used to give the user active control over the mechatronics [1]. Such approaches are also being pursued in other applications, like in the field of human-computer interaction [2], [3]. In most applications, a non-invasive detection is desired. In prosthetics a high level of reliability is also required to avoid dangerous malfunctions and increase user acceptance [4].

Electromyography (EMG) is a well-established method of detecting muscle contractions. This method uses surface electrodes to record the electrical action potentials of the contracting muscles. However, the disadvantage of this passive method is the stochastic behavior of low EMG voltages. Similar disturbances, generated by mechanical interference at the electrodes, can therefore hardly be distinguished from useful signals [5], [6]. Another electrophysiological method to detect muscle contractions is the electrical impedance myography (IMG). The IMG reduces the influence of motion artifacts, but also requires electrodes and is associated with a significantly higher electrical circuit complexity [7], [8].

In addition to the methods mentioned above, first optical approaches for muscle contraction detection, also called Optomyography (OMG), have been published in recent years. These are based on the transmission of light into the tissue using LEDs and the simultaneous detection of the reflected light using photodiodes [9]–[11]. As soon as a geometric deformation of the tissue area under consideration occurs, the optical properties and thus the transmission and reflection properties also change [12]. To not only quantify the reflected illuminance, but also to be able to make statements regarding the causes, the integration of several wavelengths is of particular interest. However, this is accompanied by the difficulty of optical multiplexing, which is typically achieved by alternately switching LEDs of different wavelengths on and off, as is known from pulse oximetry [13]. This is feasible with a small number of wavelengths. However, it is difficult to extend the method with additional LEDs, due to limitations of the switching times.

To eliminate this limitation for future systems and procedures, an alternative multiplexing method based on frequency multiplexing is presented in this work. In this approach, the currents of the light sources are controlled to generate sinusoidal signals at different frequencies. In order to avoid

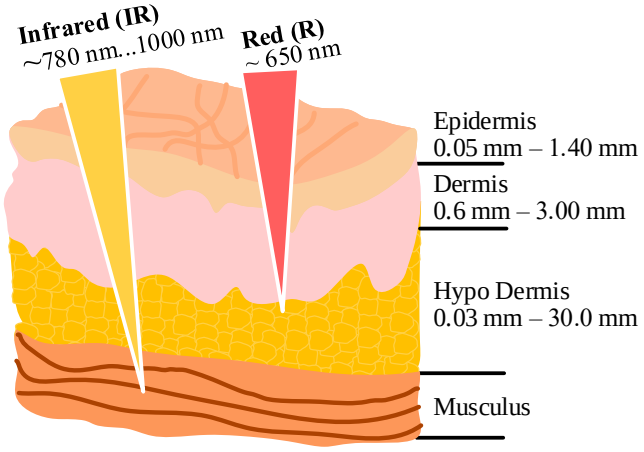

Fig. 1. Illustration of the light penetration depths into the tissue for red and infrared light, based on [14].

high sampling rates and extensive digital signal processing, the received signals are demodulated in analog form.

This work presents this new measurement approach first. Afterwards, the development of a measurement system for testing a two-wavelengths approach is explained. In the end, the functionality is tested on four subjects. The contributions of this work are threefold:

- A method for optical detection of muscle contractions.
- A measurement approach based on frequency multiplexing of light intensities that is easy to extend to multiple channels.
- First empirical functionality test on four subjects to evaluate the two-wavelengths approach.

II. Materials and Methods

A. Measurement Approach

The method presented in this work is based on wavelength-specific absorption and reflection properties of different types of tissue [14]. The layers directly below the skin surface, such as the dermis, hypodermis, and the actual muscle, are assumed to differ optically from each other. During muscular contractions, geometrical changes occur, causing temporal changes in this layer structure and thus leading to a variation of the overall optical properties of the tissue region. Previous work has already shown that significant changes in reflective properties occur during muscle contractions at least in the infrared (IR) wavelength range [9], [15]. To determine whether detectable reflection variations are actually caused by muscular contractions or by motion artifacts, the tissue should be measured simultaneously at the same location with additional wavelength information, as shown in Figure 1.

Since red (R) light also has a high penetration depth in human tissue and the red/infrared combination is already commercially available in numerous photoplethysmography (PPG) sensors, a red LED is chosen as additional light source in this work [14]. However, in terms of future multichannel measurements, the common time multiplexing of the light sources typically applied in PPG sensors limits the possible number of adjacent measurement channels due to their sampling intervals. Therefore, in this approach, the reflections of the individual light sources are separated by frequency multiplexing. This requires sinusoidal modulation of light intensities with different frequencies. To avoid distortions resulting from the non-linearity of the LEDs forward voltage while generating sinusoidal changes in light intensity, we control the LED current. The current can be assumed as nearly proportional to the LEDs light intensity within a defined control range [16], [17]. Since negative light intensities are not possible, an additional constant direct current (DC) is superimposed on the alternating current component (AC), resulting in the corresponding LED currents i_{LED} with different frequencies f_{IR} and f_{R}, as shown in equation 1.

$$i_{\mathrm{LED}}(t) = I_{\mathrm{DC}} + \hat{i}_{\mathrm{AC}} \cdot \cos(2\pi f t) \tag{1}$$

Since the relationship between the LED current and the light intensity is assumed to be linear, this results directly in the corresponding total LED light intensities ϕ_{LED}, as shown in equation 2.

$$\phi_{\mathrm{LED}}(t) = \phi_{\mathrm{DC}} + \phi_{\mathrm{AC}} \cdot \cos(2\pi f t) \tag{2}$$

The amount of light that is received by a sensor close to the LEDs depends on the effective time-dependent reflectance factor RF, which also depends on the corresponding LED wavelength. As equation 3 shows, $RF(t)$ consists of alternating RF_{AC} and direct components RF_{DC}, whereby the alternating component corresponds to the muscle contractions within a relevant frequency range of $f_{\mathrm{RF}} \leq 10\,\mathrm{Hz}$.

$$RF(t) = RF_{\mathrm{DC}} + RF_{\mathrm{AC}} \tag{3}$$

Since both wavelengths are applied simultaneously to the tissue, the measured light intensity $\phi_{\mathrm{meas.}}$ is given by equation 4.

$$\phi_{\mathrm{meas.}} = RF_{\mathrm{IR}}(t) \cdot \phi_{\mathrm{LED,IR}}(t) + RF_{\mathrm{R}}(t) \cdot \phi_{\mathrm{LED,R}}(t) \tag{4}$$

This corresponds to two amplitude modulations (AM) with the carrier frequencies of f_{IR} and f_{R} and a superimposed DC component. To extract beneficial information from this received signal, a specific signal processing chain is required.

B. Measurement Setup

A measuring system was developed that is capable of operating two separate optical channels simultaneously. The measuring system, shown in the block diagram in Figure 2, consists of an LED driver, an optical sensor and a demodulator. In addition, a PC is connected with the system via a USB Isolator (Meilhaus USB-GT MED-D) to control the LED driver and to receive the measured signals for digital signal processing and plotting. To prevent injury to the subjects, the USB Isolator conforms to the medical standard EN 60601-1 and EN 60601-2 and has a galvanic isolation protection of at least $4\,\mathrm{kV}$ potential difference between input and output [18].

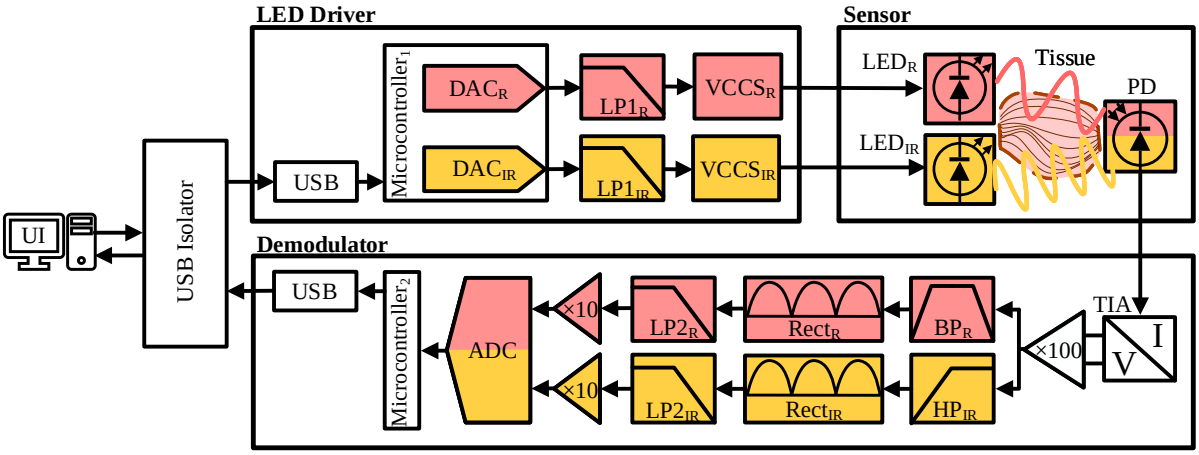

Fig. 2. Block diagram of the measurement setup.

The purpose of the LED driver, which is based on previous work, is to generate the two LED currents. LED currents are each composed of DC and corresponding AC components to distinguish channels from each other [19]. To ensure that the selected modulation frequencies are not too close to the primary signal with $f_{\mathrm{RF}} \leq 10\,\mathrm{Hz}$ and can be easily separated using analog filters, $f_{\mathrm{IR}} = 16.66\,\mathrm{kHz}$ and $f_{\mathrm{R}} = 500\,\mathrm{Hz}$ were selected. The sinusoidal signals are synthesized by the internal 12-bit digital-to-analog converters ($\mathrm{DAC_{IR}}$, $\mathrm{DAC_R}$) of $\mathrm{Microcontroller_1}$ (Microchip Technology ATSAM4S16C) with a sampling rate of $f_{\mathrm{s,DAC}} = 1\,\mathrm{Msps}$. To smooth the sampled signals, 2nd order Multiple-Feedback low-pass filters ($\mathrm{LP1_{IR}}$, $\mathrm{LP1_R}$) with a cut-off frequency of 200 kHz are applied to each channel. To convert filtered voltages to currents, voltage controlled current sources based on operational amplifiers (OPAMP) (Texas Instruments OPA552) ($\mathrm{VCCS_{IR}}$, $\mathrm{VCCS_R}$) are implemented in the Howland topology. These current sources are configured to drive the LEDs with a DC component of $I_{\mathrm{DC}} = 6\,\mathrm{mA}$ and a superimposed sinusoidal current with an amplitude of $\hat{i}_{\mathrm{AC}} = 4\,\mathrm{mA}$.

The sensor part consists of the infrared ($\mathrm{LED_{IR}}$) and red ($\mathrm{LED_R}$) light sources and a photodiode (PD) to acquire the reflected light. The Sensors dimension are $24\,\mathrm{mm} \times 20\,\mathrm{mm}$, as shown in Figure 3. The LEDs were selected according to the exposure limit values for optical radiation based on the European Directive 2006/25/EC on laser protection and the recommendations sheet of the Institute of Occupational Safety and Health of the German Social Accident Insurance for exposure limit values for skin protection [20], [21]. As mentioned above, the aim is to distinguish between interferences and signals caused by muscle contractions. Therefore, LEDs with wavelengths of different tissue penetration depths and linear current behaviour were chosen [14]. Referring to Figure 1, $\mathrm{LED_{IR}}$ (OSRAM SFH 4253) emits light with a wavelength of $\lambda_{\mathrm{IR}} = 850\,\mathrm{nm}$ and $\mathrm{LED_R}$ (Vishay VLMR 334) emits light with a wavelength of $\lambda_{\mathrm{R}} = 630\,\mathrm{nm}$ [16], [17]. The modulated reflected light from the tissue is detected and linearly converted into a photoelectric current by the PD (Luna Optoelectronics PDB-C160SM) on the sensor.

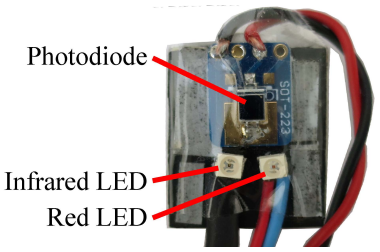

Fig. 3. Sensor board with light emitting LEDs and the acquiring photodiode.

The purpose of the demodulator block is to extract useful information from the photodiode signal and transmit it to the PC for analysis [22]. To do this, the first step is to convert the photoelectric current into a voltage signal. This is implemented with an operational amplifier (Texas Instruments AD8065) in transimpedance amplifier (TIA) topology. It is configured to convert the current into a voltage with a gain of $-1\,\mathrm{V/mA}$. Due to the very low expected photoelectric currents from the PD this voltage is amplified by a factor of -100 by an OPAMP-based inverting amplifier circuit (Texas Instruments OPA2134). Afterwards, the signal processing chain is split into two almost identical parts, one for the infrared signal component, the other for the red signal component. To extract the information of the infrared channel and to remove DC components, the signal is filtered by a second-order multiple feedback high-pass ($\mathrm{HP_{IR}}$) with a cut-off frequency of $f_{\mathrm{c,HP,IR}} = 7\,\mathrm{kHz}$. On the other hand, since the red LED is modulated with a frequency of $f_{\mathrm{R}} = 500\,\mathrm{Hz}$, the higher frequency infrared components must be eliminated, as well as the DC components. Therefore, a band-pass filter ($\mathrm{BP_R}$) is implemented, which consists of two cascaded second-order multiple feedback filters, a high-pass filter with a cut-off frequency of $f_{\mathrm{c1,BP,R}} = 100\,\mathrm{Hz}$ and a low-pass filter with a cut-off frequency of $f_{\mathrm{c2,BP,R}} = 1\,\mathrm{kHz}$. To demodulate the high-frequency signals and to extract the information of reflectivity changes, the envelopes of both the filtered signal

components are assessed by an identical cascade of rectification, smoothing and amplification. Precision rectification circuits ($\mathrm{Rect_{IR}}$, $\mathrm{Rect_R}$) for both channels are implemented using OPAMPs (Texas Instruments OPA2134) with diodes (Onsemi 1N914) in the feedback loops. Subsequently, the rectified signals are smoothed by second-order multiple feedback low-pass filters ($\mathrm{LP2_{IR}}$, $\mathrm{LP2_R}$) with a cut-off frequency of $f_{\mathrm{c,LP2}} = 10\,\mathrm{Hz}$. At the end, before digitization, the resulting envelopes are amplified by a factor of 10. The analog signals are then synchronously digitized by an analog-to-digital converter (ADC, Texas Instruments ADS131E08), which is based on previous work, with a resolution of 24 bit and a sampling rate of $f_{\mathrm{s,ADC}} = 1\,\mathrm{ksps}$. Digitized signals are transmitted through an SPI interface to $\mathrm{Microcontroller_2}$ (Microchip ATSAM4S16C), which processes the data and sends them galvanically isolated via the USB interface to the PC.

III. Results and Discussion

A. System Characterization

In this section, the measurement setup is characterized regarding the output currents, the linearity of the transmission path, the quality of channel separation, and the behavior of the precision rectifier. As measurement hardware, a 12-bit oscilloscope (Teledyne Lecroy HDO6054) is used.

First, the system is configured to generate output currents, as described in Section II-B. However, instead of driving the LEDs, the current flows through a known load resistor of $R_{\mathrm{L}} = 10\,\Omega$ and the resulting voltage drop is measured through the oscilloscope. The maximum error in amplitude of the output current is below 5 %, which mainly results from component tolerances and is within an acceptable range.

For the characterization of the transmission path including the optoelectronic components, the amplitudes of the high-frequency carrier signals and the first two harmonic frequencies at the output of the TIA are measured. During the measurement, the optical sensor board is placed above a bright reflective surface. The measurements in Table I show that the harmonic signal components are at least $-44.7\,\mathrm{dB}$ below the corresponding carrier signals, which indicates a high linearity of the transmission path.

TABLE I
Harmonic distortion of the TIAs output voltage during a dual-channel light transmission

ID	f/kHz	Carrier Freq./dB	1.Harmonic/dB	2.Harmonic/dB
TIA	0.5	9.1	< -40	< -40
TIA	16.66	5.2	-39.5	-52.9

Operating in the same measurement setup, the crosstalks between both channels are measured at the outputs of $\mathrm{HP_{IR}}$ and $\mathrm{BP_R}$ in Table II. Using the oscilloscope, it was determined to be below $-47\,\mathrm{dB}$, which is acceptable in this application. The signal losses of the precision rectifiers are measured at the outputs of $\mathrm{Rect_{IR}}$ and $\mathrm{Rect_R}$. The results in Table III show that an amplitude attenuation of 21.9 % occurs at a signal frequency of $16.66\,\mathrm{kHz}$. The loss is acceptable for implementations with two channels like in this paper, but must be taken into account and optimized for conversions with more than two LED channels where higher frequencies are applied for the channel separation.

TABLE II
Crosstalks between the R and IR channel behind $\mathrm{BP_R}$ and $\mathrm{HP_{IR}}$ during a dual-channel light transmission

ID	f/kHz	Red/dB	IR/dB
$\mathrm{BP_R}$	0.5	0	-56
$\mathrm{HP_{IR}}$	16.66	-47	0

TABLE III
Amplitude attenuation of the Rectifiers during a single-channel light transmission

ID	$2 \cdot$ f/kHz	$\hat{u}_{\mathrm{in}}$/mV	$\hat{u}_{\mathrm{out}}$/mV	Δu/%
$\mathrm{Rect_R}$	$2 \cdot 0.5$	345	325	5.8
$\mathrm{Rect_{IR}}$	$2 \cdot 16.66$	320	250	21.9

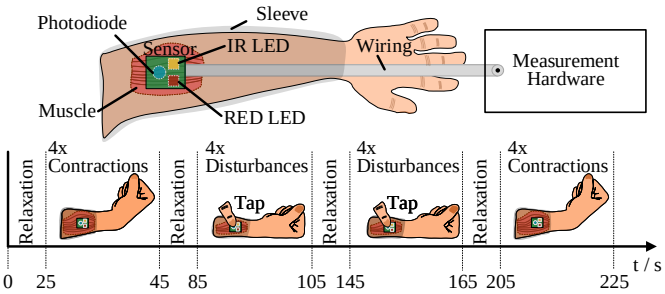

Fig. 4. Experimental procedure to validate the measurement setup for muscle contraction detection.

B. Subject Measurements

To evaluate the new approach, measurements are performed on four healthy subjects. The subject measurements presented in this manuscript were approved by the Ethics Committee of the University of Lübeck (01-04-2020). In the test set-up chosen, the optical sensor board is placed on the skin of the forearm above the brachioradialis muscle, as shown in Figure 4. It is fixed with a forearm sleeve (Vertics Vertics.Sleeves) to ensure constant contact pressure and is connected to the measurement hardware. The measurement is performed according to the diagram depicted in Figure 4.

The protocol is divided into four phases. In the first measurement phase, the subject relaxes the arm for a duration of 25 s. Then the muscle is contracted 4 times for about 2 s each. In the second measurement phase, the subject relaxes the arm for a duration of 40 s, followed by a disturbance phase of 20 s in which the optical sensor board is press four times $\approx 5\,\mathrm{mm}$ into the tissue. The third phase is equal to the second phase. After further 40 s relaxing time, the muscle is again contracted 4 times for about 2 s each.

The acquired signals are shown in Figure 5. For better visualization, the signals were normalized.

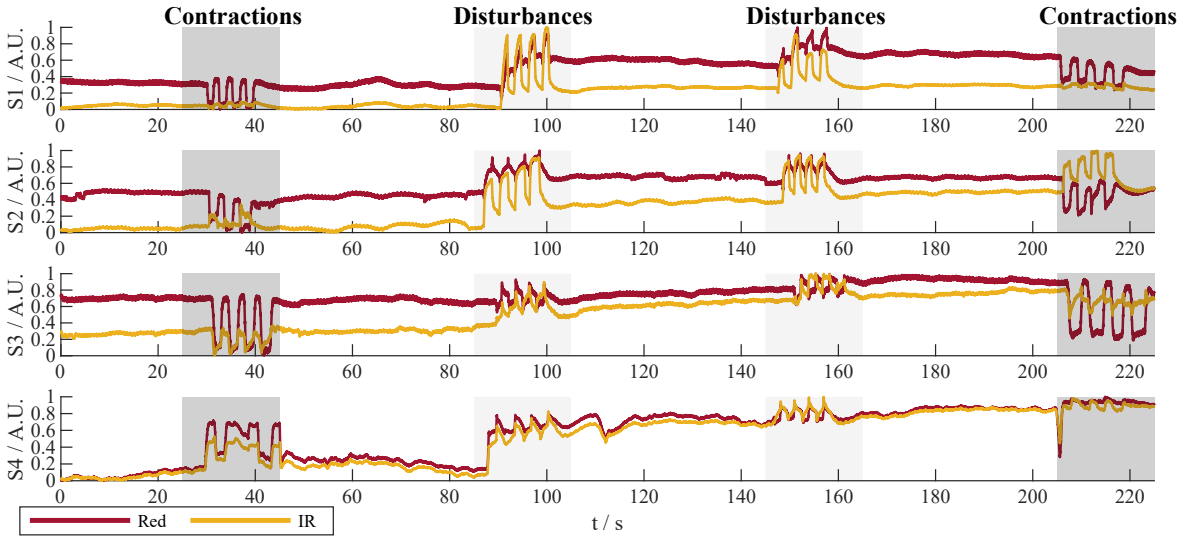

Fig. 5. Measurement results of four subjects while muscle contractions and disturbances.

The measurement results show that it is possible to record muscle contractions under laboratory conditions using a two wavelengths optical sensor measurement setup. Especially, in the signals from the subjects S1, S2 and S3 the contractions are clearly indicated by significant decreases in the red signals. As expected the disturbances are also clearly present in the red signals. The behavior of the infrared signals is similar but differs in some situations from the red signal and could therefore be helpful to distinguish between an actual contraction and a disturbance. However, this differentiation does not seem to work reliably. Another approach of analysis is based on focusing on the strength of signal changes. The results show that especially the red signal changes significantly during a contraction and the infrared signal seems to be more sensitive to disturbances.

IV. Conclusions

In this work, a new measurement approach for optical detection of muscle contractions was presented. The principle is based on two light sources with separated wavelengths to distinguish between actual muscle contractions and motion artifacts. After the introduction of the measurement system, first subject measurements were presented. The measurements demonstrated the functionality of the measurement setup and the capability of detecting muscle contractions as well as motion artifacts. First examinations indicate that the simultaneous measurement with infrared and red wavelength provides additional information in comparison to single-wavelength measurements. Further studies are planned as the limited subject measurements does not provide sufficient data for a comprehensive analysis. The system is limited to two static wavelengths. We will conduct further investigations to identify the optimal combination of wavelengths for our application. Additionally, our plan involves extending the measurement approach by incorporating EMG measurements to enhance the OMG procedure with additional reference data. By combining both methods, we can explore more sophisticated data analysis techniques to differentiate disturbances from muscle contractions with greater precision.

Acknowledgment

This work was funded by the Joachim Herz Stiftung under the project PASBADIA. The preliminary work for this project was supported by the German Federal Ministry of Education and Research (BMBF) under the project INOPRO (FKZ16SV7666). Horst Hellbrück is adjunct professor at the Institute of Telematics of University of Lübeck.

References

[1] Y. Fang, N. Hettiarachchi, D. Zhou, and H. Liu, "Multi-modal sensing techniques for interfacing hand prostheses: A review," *IEEE Sensors Journal*, vol. 15, no. 11, pp. 6065–6076, Nov. 2015.

[2] M. Simao, N. Mendes, O. Gibaru, and P. Neto, "A review on electromyography decoding and pattern recognition for human-machine interaction," *IEEE Access*, vol. 7, pp. 39 564–39 582, 2019.

[3] J. Qi, G. Jiang, G. Li, Y. Sun, and B. Tao, "Intelligent human-computer interaction based on surface emg gesture recognition," *IEEE Access*, vol. 7, pp. 61 378–61 387, 2019.

[4] A. Cisnal, J. Perez-Turiel, J.-C. Fraile, D. Sierra, and E. de la Fuente, "Robhand: A hand exoskeleton with real-time emg-driven embedded control. quantifying hand gesture recognition delays for bilateral rehabilitation," *IEEE Access*, vol. 9, pp. 137 809–137 823, 2021.

[5] B. R. Schlink, A. D. Nordin, and D. P. Ferris, "Comparison of signal processing methods for reducing motion artifacts in high-density electromyography during human locomotion," *IEEE Open Journal of Engineering in Medicine and Biology*, vol. 1, pp. 156–165, 2020.

[6] R. Chowdhury, M. Reaz, M. Ali, A. Bakar, K. Chellappan, and T. Chang, "Surface electromyography signal processing and classification techniques," *Sensors*, vol. 13, no. 9, pp. 12 431–12 466, sep 2013.

[7] S. B. Rutkove, "Electrical impedance myography: Background, current state, and future directions," *Muscle and Nerve*, vol. 40, no. 6, pp. 936–946, dec 2009.

[8] R. Kusche, A. Oltmann, and P. Rostalski, "A wearable dual-channel bioimpedance spectrometer for real-time muscle contraction detection," *IEEE Sensors Journal*, pp. 1–1, 2024.

[9] H. H. Muhammed and R. Jammalamadaka, "A new approach for rehabilitation and upper-limb prosthesis control using optomyography (omg)," in *2016 1st International Conference on Biomedical Engineering (IBIOMED)*. IEEE, Oct. 2016.

[10] H. H. Muhammed and J. Raghavendra, "Optomyography (omg) : A novel technique for the detection of muscle surface displacement using photoelectric sensors," in *Measurements - Proceedings of the 10th International Conference on Bioelectromagnetism, International Society for Bioelectromagnetism*, 2015.

[11] T. Bianchi, D. Zambarbieri, G. Beltrami, and G. Verni, "NIRS monitoring of muscle contraction to control a prosthetic device," in *Biomedical Sensors, Fibers, and Optical Delivery Systems*, F. Baldini, N. I. Croitoru, M. Frenz, I. Lundstroem, M. Miyagi, R. Pratesi, and O. S. Wolfbeis, Eds. SPIE, Jan. 1999.

[12] A. Chianura and M. E. Giardini, "An electrooptical muscle contraction sensor," *Medical & Biological Engineering & Computing*, vol. 48, no. 7, pp. 731–734, May 2010.

[13] D. Ray, T. Collins, S. Woolley, and P. Ponnapalli, "A review of wearable multi-wavelength photoplethysmography," *IEEE Reviews in Biomedical Engineering*, vol. 16, pp. 136–151, 2023.

[14] P. Taroni, A. Pifferi, A. Torricelli, D. Comelli, and R. Cubeddu, "In vivo absorption and scattering spectroscopy of biological tissues," *Photochemical and Photobiological Sciences*, vol. 2, no. 2, pp. 124–129, Feb. 2003.

[15] A. Chianura and M. E. Giardini, "An electrooptical muscle contraction sensor," *Medical and Biological Engineering and Computing*, vol. 48, no. 7, pp. 731–734, May 2010.

[16] OSRAM, *SFH 4253*, Datasheet, Aug. 2020, rev. 1.6.

[17] Vishay Semiconductors, *VLMR 334 - Power SMD LED PLCC-2*, Datasheet, Jul. 2019, rev. 1.2.

[18] Meilhaus Electronic GmbH, *USB-GT Interface Isolator*, Manual, Nov. 2019, rev. 3.

[19] R. Kusche, S. Hauschild, and M. Ryschka, "Galvanically decoupled current source modules for multi-channel bioimpedance measurement systems," *Electronics*, vol. 6, no. 4, p. 90, Oct. 2017.

[20] M. Brose, H. Brüggenmeyer, M. Graf, W. Horak, H. Jossen, G. Ott, H.-D. Reidenbach, H. Siekmann, M. Steinmetz, E. Sutter, and D. Weiskopf, "Leitfaden sichtbare und infrarote strahlung," Dec. 2011.

[21] ZSV, "Directive 2006/25/ec of the european parliament and of the council of 5 april 2006 on the minimum health and safety requirements regarding the exposure of workers to risks arising from physical agents (artificial optical radiation) (19th individual directive within the meaning of article 16(1) of directive 89/391/eec)," EU-Directive, 2006, version: 07/2019.

[22] R. Kusche, P. Klimach, and M. Ryschka, "A multichannel real-time bioimpedance measurement device for pulse wave analysis," *IEEE Transactions on Biomedical Circuits and Systems*, vol. 12, no. 3, pp. 11 687–11 696, jun 2018.